

## General construction scheme for geometrically nontrivial flat band models

Hyeongseop Kim <sup>1</sup>, Chang-geun Oh<sup>2</sup> & Jun-Won Rhim <sup>1,3</sup>✉

A singular flat band (SFB), a distinct class of the flat band, has been shown to exhibit various intriguing material properties characterized by the quantum distance. We present a general construction scheme for a tight-binding model hosting an SFB, where the quantum distance profile can be controlled. We first introduce how to build a compact localized state (CLS), endowing the flat band with a band-touching point and a specific value of the maximum quantum distance. Then, we develop a scheme designing a tight-binding Hamiltonian hosting an SFB starting from the obtained CLS, with the desired hopping range and symmetries. We propose several simple SFB models on the square and kagome lattices. Finally, we establish a bulk-boundary correspondence between the maximum quantum distance and the boundary modes for the open boundary condition, which can be used to detect the quantum distance via the electronic structure of the boundary states.

<sup>1</sup>Department of Physics, Ajou University, Suwon 16499, Korea. <sup>2</sup>Department of Applied Physics, The University of Tokyo, Tokyo 113-8656, Japan. <sup>3</sup>Research Center for Novel Epitaxial Quantum Architectures, Department of Physics, Seoul National University, Seoul 08826, Korea. ✉email: [jwrhim@ajou.ac.kr](mailto:jwrhim@ajou.ac.kr)

When a band has a macroscopic degeneracy, we call it a flat band<sup>1,2</sup>. Flat band systems have received great attention because their van Hove singularity is expected to stabilize various many-body states when the Coulomb interaction is introduced. Examples of such correlated states induced by flat bands are unconventional superconductivity<sup>3–11</sup>, ferromagnetism<sup>12–18</sup>, Wigner crystal<sup>19–21</sup>, and fractional Chern insulator<sup>22–31</sup>. Recently, it was revealed that the flat band could be nontrivial from the perspective of geometric notions, such as the quantum distance, quantum metric, and cross-gap Berry connection<sup>32–36</sup>. The quantum distance is related to the resemblance between two quantum states defined by

$$d^2 = 1 - |\langle \psi_1 | \psi_2 \rangle|^2, \quad (1)$$

which is positive-valued and ranging from 0 to 1<sup>37–39</sup>. If a flat band has a band-touching point with another parabolic band and the maximum value of the quantum distance, denoted by  $d_{\max}$ , between eigenvectors around the touching point, is nonzero, we call it a singular flat band (SFB)<sup>40</sup>. The SFB hosts non-contractible loop states featuring exotic topological properties in real space<sup>41,42</sup>. The Landau level structure of the SFB is shown to be anomalously spread into the band gap region<sup>32,33</sup>, and the maximum quantum distance determines the magnitude of the Landau level spreading. Moreover, if we introduce an interface in the middle of an SFB system by applying different electric potentials, an interface mode always appears, and the maximum quantum distance determines its effective mass<sup>43</sup>.

Diverse unconventional phenomena characterized by quantum distance are expected to occur in the SFB systems. However, we lack good tight-binding models hosting the SFB where one can control the quantum distance, although numerous flat band construction methods have been developed<sup>44–52</sup>. This paper suggests a general construction scheme for the tight-binding Hamiltonians with an SFB and the controllable maximum quantum distance. The construction process's essential part is designing a compact localized state (CLS), which gives the desired maximum quantum distance. The CLS is a characteristic eigenstate of the flat band, which has finite amplitudes only inside a finite region in real space<sup>40</sup>. The CLS can be transformed into the Bloch eigenstate, and any Hamiltonian having this as one of the eigenstates must host a flat band<sup>40</sup>. Among infinitely many possible tight-binding Hamiltonians for a given CLS, one can choose several ones by implementing the wanted symmetries and hopping range into the construction scheme. Using the construction scheme, we suggest several simple tight-binding models hosting an SFB characterized by the maximum quantum distance on the square and kagome lattices. Using the obtained tight-binding models, we propose a bulk-boundary correspondence of the flat band system from the maximum quantum distance to address the question of how to measure the maximum quantum distance in experiments. The previous work established the bulk-interface correspondence for the interface between two domains with different electric potentials in the same SFB system, where the maximum quantum distance of the bulk determines the interface mode's effective mass<sup>43</sup>. We show that the same correspondence applies to open boundaries if a boundary mode exists.

## Results

**General flat band construction scheme.** Since the key ingredient of the flat band construction scheme is designing a CLS, we begin with a brief review of it. The general form of the Bloch wave

function of the  $n$ -th band with momentum  $\mathbf{k}$  is given by

$$|\psi_{n,\mathbf{k}}\rangle = \frac{1}{\sqrt{N}} \sum_{\mathbf{R}} \sum_{q=1}^Q e^{i\mathbf{k}\cdot\mathbf{R}} v_{n,\mathbf{k},q} |\mathbf{R}, q\rangle, \quad (2)$$

where  $N$  is the number of unit cells in the system,  $\mathbf{R}$  represents the position vectors of the unit cells,  $|\mathbf{R}, q\rangle$  corresponds to the  $q$ -th orbital among  $Q$  orbitals in a unit cell, and  $v_{n,\mathbf{k},q}$  is the  $q$ -th component of the eigenvector  $\mathbf{v}_{n,\mathbf{k}}$  of the  $Q \times Q$  Bloch Hamiltonian<sup>53</sup>. Then it was shown that if the  $n_0$ -th band is flat, one can always find a linear combination of the Bloch wave functions resulting in the CLS of the form:

$$|\chi_{\mathbf{R}}\rangle = c_{\chi} \sum_{\mathbf{k} \in \text{BZ}} \sum_{q=1}^Q \alpha_{\mathbf{k}} v_{n_0,\mathbf{k},q} e^{i\mathbf{k}\cdot(\mathbf{R}-\mathbf{R}')} |\mathbf{R}', q\rangle, \quad (3)$$

where  $c_{\chi}$  is the normalization constant and  $\alpha_{\mathbf{k}}$  is a mixing coefficient of the linear combination<sup>40</sup>. It is important to note that  $\alpha_{\mathbf{k}} v_{n_0,\mathbf{k},q}$  is a finite sum of exponential factors  $e^{i\mathbf{k}\cdot\mathbf{R}}$  so that the range of  $\mathbf{R}'$  in (3) with the nonzero coefficient of  $|\mathbf{R}', q\rangle$  is finite. If  $\alpha_{\mathbf{k}} v_{n_0,\mathbf{k},q} = 0$  at  $\mathbf{k} = \mathbf{k}_0$  for all kinds of  $\alpha_{\mathbf{k}}$  satisfying the above properties, we call the band the SFB because  $v_{n_0,\mathbf{k},q}$  becomes discontinuous at  $\mathbf{k}_0$  in this case. From (3), one can note that the constants in front of each exponential factor of  $\alpha_{\mathbf{k}} v_{n_0,\mathbf{k},q}$  becomes the amplitude of the CLS.

We construct a flat band Hamiltonian from a CLS arbitrarily designed on a given lattice. This part corresponds to the third and fourth stages of the construction scheme sketched in Fig. 1. By using the correspondence between the CLS and Bloch eigenvector in (3), one can obtain  $\alpha_{\mathbf{k}} v_{n_0,\mathbf{k},q}$  in the form of the finite sum of exponential factors from the designed CLS. Then, by normalizing  $\alpha_{\mathbf{k}} v_{n_0,\mathbf{k},q}$ , one can have the flat band's eigenvector  $v_{n_0,\mathbf{k},q}$  corresponding to the CLS. Our purpose is to find a tight-binding Hamiltonian of the form

$$H_{ij}^{\text{lattice}}(\mathbf{k}) = \sum_{\Delta\mathbf{R}} t_{ij}(\Delta\mathbf{R}) e^{-i\mathbf{k}\cdot\Delta\mathbf{R}}, \quad (4)$$

which satisfies

$$[H_{ij}^{\text{lattice}}(\mathbf{k}) - E_{\text{flat}}] \alpha_{\mathbf{k}} \mathbf{v}_{n_0,\mathbf{k}} = 0, \quad (5)$$

where  $E_{\text{flat}}$  is the flat band's energy and  $\mathbf{v}_{n_0,\mathbf{k}}$  is a column vector with components  $v_{n_0,\mathbf{k},q}$ . Here,  $t_{ij}(\Delta\mathbf{R})$  represents the hopping parameter between the  $i$ th and  $j$ th orbitals in unit cells separated by  $\Delta\mathbf{R} = \sum_{\nu=1}^d n_{\nu} \mathbf{a}_{\nu}$ , where  $n_{\nu}$  is an integer,  $d$  is spatial

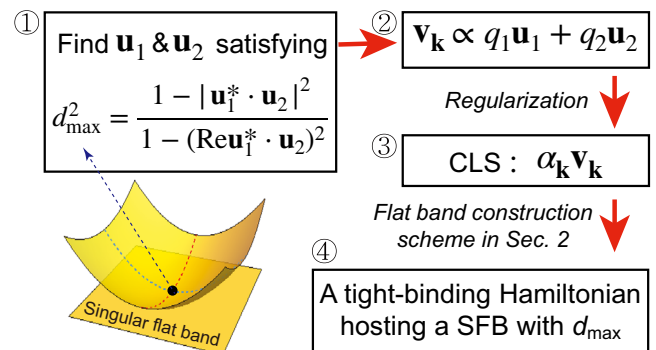


**Fig. 1 The SFB construction scheme overview.** A scheme for the construction of a tight-binding model hosting a singular flat band (SFB) characterized by the maximum quantum distance ( $d_{\max}$ ). First, we find two vectors with complex components to yield the desired  $d_{\max}$ . Then, we build a compact localized state (CLS) from the two vectors in the second and third steps. Finally, we obtain an SFB Hamiltonian from the CLS using the general flat band construction scheme.

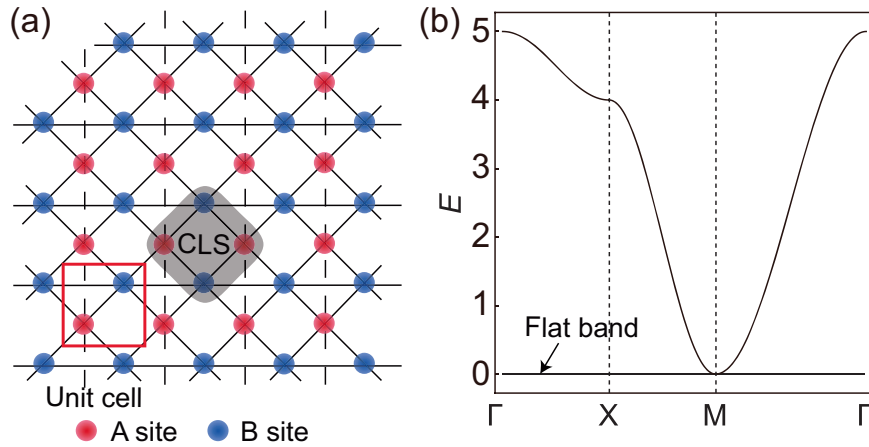


**Fig. 2** The checkerboard lattice model  $\text{CB}_1$ . **a** A red box represents the unit cell. The hopping amplitudes are 1 for the dashed lines along the  $y$  axis,  $-a/b$  for black solid lines along diagonal directions, and  $a^2/b^2$  for the black solid lines along the  $x$  axis. The compact localized state (CLS) corresponding to the flat band is drawn by a gray region. The CLS's amplitudes are  $a$  at the A-sites and  $b$  at the B-sites. **b** The band structure of the checkerboard model for  $a = 1$  and  $b = 2$ .

dimension, and  $\mathbf{a}_\nu$  is the primitive vector. For convenience, we denote  $t_{ij}^{n_1, n_2, \dots, n_\nu} \equiv t_{ij}(\Delta\mathbf{R})$  and  $e_\nu \equiv e^{-i\mathbf{k} \cdot \mathbf{a}_\nu}$ . We use a bar notation for the complex conjugate such that  $\overline{t_{ij}^{n_1, n_2, \dots, n_\nu}} = (t_{ij}^{n_1, n_2, \dots, n_\nu})^*$  and  $\overline{e_\nu} = (e_\nu)^*$ . Then, the matrix element of the tight-binding Hamiltonian is rewritten as

$$H_{ij}^{\text{lattice}}(\mathbf{k}) = \sum_{n_1, n_2, \dots, n_\nu} \sum_{ij} t_{ij}^{n_1, n_2, \dots, n_\nu} \prod_{\nu'} e_{\nu'}^{n_{\nu'}}. \quad (6)$$

Here, the hopping parameters  $t_{ij}^{n_1, n_2, \dots, n_\nu}$  can be considered complex unknowns determined by the matrix equation in (5). One can encode some wanted hopping range and symmetries by manipulating the number of unknown hopping parameters and setting relations between them, respectively. Noting that  $\alpha_{\mathbf{k}} \mathbf{v}_{n_0, \mathbf{k}} = \sum_{n_1, n_2, \dots, n_\nu} c_{n_1, n_2, \dots, n_\nu} \prod_{\nu'} e_{\nu'}^{n_{\nu'}}$  as described above, the matrix equation (5) leads to a system of linear equations obtained from the coefficients of the independent exponential factors.

Let us consider a simple example, the flat band Hamiltonian on the checkerboard lattice, which is illustrated in Fig. 2a. We design a CLS in the shape of a square represented by a gray region in Fig. 2a, having amplitudes  $a$  and  $b$  on the A and B sites, respectively. From the CLS, one can obtain the flat band's eigenvector  $\alpha_{\mathbf{k}} \mathbf{v}_{n_0, \mathbf{k}}$  in momentum space such that the CLS's amplitude in the unit cell  $\Delta\mathbf{R} = \sum_{\nu=1}^d n_\nu \mathbf{a}_\nu$  becomes the coefficient of the exponential factor  $\prod_{\nu'} e_{\nu'}^{n_{\nu'}}$ . As a result, we have

$$\alpha_{\mathbf{k}} \mathbf{v}_{n_0, \mathbf{k}} = \begin{pmatrix} a + a e_1 \\ b + b \overline{e_2} \end{pmatrix}. \quad (7)$$

The next step is to design the tight-binding Hamiltonian (6). We seek one with real-valued hopping parameters up to the next-nearest hopping range. Then, the matrix elements of  $H^{\text{CB}_1}$  are of the form

$$H_{11}^{\text{CB}_1} = t_{11}^{0,0} + t_{11}^{0,-1} \overline{e_2} + t_{11}^{0,1} e_2, \quad (8)$$

$$H_{12}^{\text{CB}_1} = t_{12}^{0,0} + t_{12}^{1,0} e_1 + t_{12}^{0,1} e_2 + t_{12}^{1,1} e_1 e_2, \quad (9)$$

$$H_{22}^{\text{CB}_1} = t_{22}^{0,0} + t_{22}^{-1,0} \overline{e_1} + t_{22}^{1,0} e_1, \quad (10)$$

From the flat band condition (5) and by enforcing the hermiticity, one can find relationships between the tight-binding parameters, which lead to the following form of the Hamiltonian:

$$H^{\text{CB}_1} = \begin{pmatrix} -2(1 + \cos k_y) & \frac{a}{b}(1 + e_1)(1 + e_2) \\ \frac{a}{b}(1 + \overline{e_1})(1 + \overline{e_2}) & -\frac{2a^2}{b^2}(1 + \cos k_x) \end{pmatrix}, \quad (11)$$

where we further assume that  $a$  and  $b$  are real constants and  $t_{11}^{0,0} = -2$  for convenience. This Hamiltonian yields a zero-energy flat band and lower parabolic with a singular band-touching point at  $\mathbf{k} = (\pi, \pi)$  as plotted in Fig. 2b. In fact, this band-crossing is already designed at the construction stage of the CLS in (7) by assigning a simultaneous zero of all the components of  $\alpha_{\mathbf{k}} \mathbf{v}_{n_0, \mathbf{k}}$  at  $\mathbf{k} = (\pi, \pi)$ .

**Maximum quantum distance.** In this section, we discuss how to endow the band-crossing of the flat band with the wanted value of the maximum quantum distance  $d_{\text{max}}$  when we construct a flat band model. Specifically, the quantum distance between two Bloch eigenstates with momenta  $\mathbf{k}$  and  $\mathbf{k}'$  is denoted as  $d(\mathbf{k}, \mathbf{k}')^2 = 1 - |\mathbf{v}_{\mathbf{k}'}^* \cdot \mathbf{v}_{\mathbf{k}}|^2$  and  $d_{\text{max}}$  is defined as

$$d_{\text{max}}^2 = \lim_{r_D \rightarrow 0} \max \left[ d(\mathbf{k}, \mathbf{k}')^2 \right] \Big|_{\mathbf{k}, \mathbf{k}' \in D(\mathbf{k}_0)}, \quad (12)$$

where  $\mathbf{v}_{\mathbf{k}}$  is the flat band's eigenvector and  $D(\mathbf{k}_0)$  is a closed disk with radius  $r_D$  centered at the band-crossing point  $\mathbf{k}_0$ <sup>32</sup>. In the previous study,  $d_{\text{max}}$  was proposed to measure the strength of the singularity at  $\mathbf{k}_0$ . The finite  $d_{\text{max}}$  also indicates the divergence of the Fubini-Study metric<sup>54</sup> defined by the real part of the quantum geometric tensor  $Q_{\mu\nu} = \langle \partial_\mu \psi | \partial_\nu \psi \rangle - \langle \partial_\mu \psi | \psi \rangle \langle \psi | \partial_\nu \psi \rangle$ . For the generic SFB Hamiltonian characterized by  $d_{\text{max}}$ , the quantum geometric tensor is evaluated as

$$Q_{\text{SFB}}(\mathbf{k}) = \frac{d_{\text{max}}^2}{4m_1 m_2 E_{\text{para}}(\mathbf{k})^2} \begin{pmatrix} k_x^2 & k_x k_y \\ k_x k_y & k_y^2 \end{pmatrix}, \quad (13)$$

where  $E_{\text{para}}(\mathbf{k}) = 2t_1 k_x^2 + 2t_2 k_x k_y + (2t_3 + t_4^2/t_1) k_y^2$  is the energy of the parabolic band touching with the SFB, and  $m_1$  and  $m_2$  are the minimum and maximum effective mass it [See Supplementary Note 1 for details]. While the real and imaginary parts of the quantum geometric tensor correspond to the quantum metric and the Berry curvature, respectively, the Berry curvature vanishes for all momenta so that the Fubini-Study metric is identical to the quantum geometric tensor in the SFB. Since  $E_{\text{para}}(\mathbf{k}) \propto k^2$ , where  $k = \sqrt{k_x^2 + k_y^2}$ , every element of the Fubini-Study metric

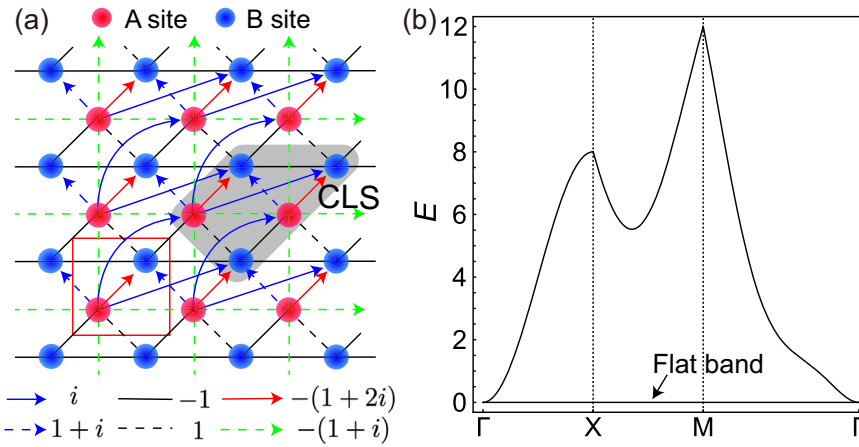


**Fig. 3 The checkerboard lattice model  $CB_2$ .** **a** The checkerboard flat band model with the maximum quantum distance  $d_{\max} = 1/\sqrt{2}$ . A red box represents the unit cell. The hopping parameters are given below the lattice structure. For the complex hopping processes, the hopping direction is represented by the arrow. The gray region stands for the compact localized state (CLS). **b** The band structure of the checkerboard model  $CB_2$ .

diverges algebraically ( $\sim 1/k^2$ ) approaching the band-crossing point at  $\mathbf{k} = 0$ . This singularity disappears if  $d_{\max}$  becomes zero because the Fubini-Study metric simply vanishes in this case. Note that if there is a singularity at the touching point, the quantum distance between the Bloch eigenstates can remain finite even if the momenta of them are very close to  $\mathbf{k}_0$ <sup>32</sup>. For the well-known SFB models, such as the kagome and checkerboard lattice models,  $d_{\max}$  is found to be unity. While  $0 \leq d_{\max} \leq 1$  in general<sup>32</sup>, there have been almost no examples of the tight-binding models hosting  $d_{\max}$  smaller than 1.

One can design  $\mathbf{v}_k$  of the flat band to have a specific value of  $d_{\max}$  by manipulating the form of the linear expansion of  $\alpha_k \mathbf{v}_k$  around the band-crossing point. Denoting  $q_\mu = k_\mu - k_{0,\mu}$ , where  $\mathbf{k}_0$  is the band-crossing point, the eigenvector  $\alpha_k \mathbf{v}_k$  can be written as

$$\alpha_k \mathbf{v}_k \simeq q_1 \mathbf{u}_1 + q_2 \mathbf{u}_2, \tag{14}$$

in the vicinity of  $\mathbf{k}_0$  up to the linear order of  $\mathbf{q}$ . Here,  $\mathbf{u}_1$  and  $\mathbf{u}_2$  are  $Q \times 1$  constant normalized vectors. Then, one can show that

$$d_{\max}^2 = \frac{1 - |\mathbf{u}_1^* \cdot \mathbf{u}_2|^2}{1 - (\text{Re} \mathbf{u}_1^* \cdot \mathbf{u}_2)^2}. \tag{15}$$

See Supplementary Note 2 for the detailed derivations. By using this relationship, one can choose two constant vectors  $\mathbf{u}_1$  and  $\mathbf{u}_2$ , giving the desired value of  $d_{\max}$ . Then, performing a regularization of (14) by applying transformations, such as  $q_i \rightarrow \sin q_i$  and  $q_i \rightarrow 1 - e^{iq_i}$ , one can obtain  $\alpha_k \mathbf{v}_k$ , the Fourier transform of a CLS, in the form of a finite sum of exponential factors  $e_v$  and  $\bar{e}_v$ . In this stage, corresponding to the first to third steps in Fig. 1, one can control the size of the CLS, which is closely related to the hopping range of the tight-binding model obtained from this CLS. While the regularization process contains a large degree of arbitrariness for the final tight-binding model, this arbitrariness can be reduced quite much if we select CLSs with a size as small as possible. Once we obtain  $\alpha_k \mathbf{v}_k$ , the tight-binding Hamiltonian with the desired  $d_{\max}$  can be built by using the construction scheme in the previous section.

From the  $d_{\max}$ -formula (15), one can note that  $d_{\max}$  can be less than one and larger than zero only when  $\mathbf{u}_1^* \cdot \mathbf{u}_2$  is not real or pure imaginary. Namely,  $u_{1,m}^* u_{2,m}$  should be imaginary at least for one  $m$ , where  $u_{i,m}$  is the  $m$ -th component of  $\mathbf{u}_i$ . Let us denote such an index  $m$  by  $m_0$ . Then, the  $m_0$ -th component of  $\alpha_k \mathbf{v}_k$ , given by  $\alpha_k \mathbf{v}_k|_{m_0} = u_{1,m_0} q_1 + u_{2,m_0} q_2$ , must be regularized into a form, where the coefficients of the exponential factors contain both the real and imaginary values. This implies that the CLS

corresponding to the SFB with  $0 < d_{\max} < 1$  cannot be constructed only with the real amplitudes. Note that the CLS of the flat band of the kagome lattice can be represented by only real amplitudes because the corresponding  $d_{\max}$  is unity. However, the CLS should consist of different complex amplitudes in at least two atomic sites for generic flat bands with  $0 < d_{\max} < 1$ . The tight-binding Hamiltonian stabilizing such a CLS usually requires complex hopping parameters. Moreover, it is shown in Methods that we need more than two exponential factors for at least one component of  $\alpha_k \mathbf{v}_k$ . This implies that we usually need hopping processes between atoms at a longer distance than the nearest-neighbor ones.

Let us consider the checkerboard lattice example again. We assume that the touching point is at  $\mathbf{k} = (0, 0)$ . First, to obtain a model with  $d_{\max} = 1$ , we can choose  $\mathbf{u}_1 = (i, 0)^T$  and  $\mathbf{u}_2 = (0, -i)^T$  in (14), using the formula (15). Then, we apply the regularization  $ik_1 \rightarrow 1 - e^{-ik_1}$  and  $ik_2 \rightarrow 1 - e^{ik_2}$  to obtain the CLS's Fourier transform. Second, on the other hand, one can let the CLS have  $d_{\max} = 1/\sqrt{2}$  by choosing  $\mathbf{u}_1 = (i, -1)^T/\sqrt{2}$  and  $\mathbf{u}_2 = (0, -i)^T$ . In this case, an example of the regularization gives  $\alpha_k \mathbf{v}_k = (1 - e^{-ik_1}, 1 + i - ie^{-ik_1} - e^{ik_2})^T$ . The CLS corresponding to this eigenvector is drawn in Fig. 3a. An example of the flat band tight-binding Hamiltonian obtained from this choice of the CLS is given by

$$H^{CB_2} = \begin{pmatrix} v_2 v_2^* & -v_1 v_2^* \\ -v_2 v_1^* & v_1 v_1^* \end{pmatrix}, \tag{16}$$

where  $v_1 = 1 - e^{-ik_1}$  and  $v_2 = 1 + i - ie^{-ik_1} - e^{ik_2}$ . The band structure of this model is shown in Fig. 3b. One can note that the band has nonzero slopes at X and M points due to the broken time-reversal, mirror, and inversion symmetries. As discussed above, the CLS contains both the real and imaginary amplitudes, and the Hamiltonian possesses imaginary hopping processes in the  $d_{\max} = 1/\sqrt{2}$  case.

**Flat band models characterized by the quantum distance.** We first construct a simple tight-binding model hosting an SFB characterized by  $d_{\max}$  in the kagome lattice as shown in Fig. 4a, b. When we consider only the nearest-neighbor hopping processes in the kagome lattice, which is the most popular case, the flat band already has a quadratic band-touching, but the corresponding  $d_{\max}$  is fixed to 1<sup>32</sup>. We generalize this conventional kagome lattice model so that  $d_{\max}$  can vary by adding some next-nearest-neighbor hopping processes.

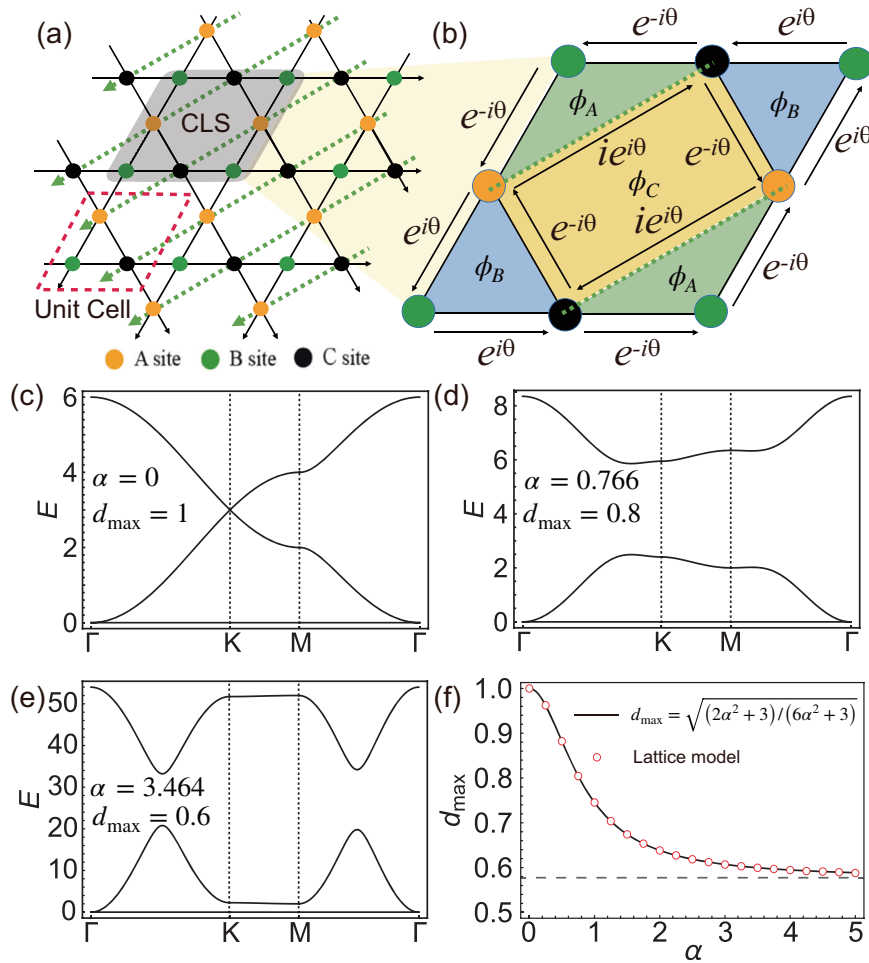


**Fig. 4 The kagome lattice model characterized by the quantum distance.** **a** The nearest and the next-nearest-neighbor hopping processes are denoted by the black solid and green dashed lines, respectively. The compact localized state (CLS) corresponding to the flat band of this model is represented by the gray region. **b** The phase parts of the hopping parameters are highlighted. The magnetic fluxes for the complex hopping parameters are given by  $\phi_A = \pi/2 - \theta$ ,  $\phi_B = \theta$ , and  $\phi_C = -\pi$ . **c–e** Band dispersions for  $\alpha = 0$ ,  $\alpha = 0.766$ , and  $\alpha = 3.464$ , where  $\theta = \cos^{-1}(1/\sqrt{1 + \alpha^2})$ . **f** The maximum quantum distance  $d_{max}$  as a function of  $\alpha$ . The formula (17) drawn by a black curve is compared with the numerically calculated  $d_{max}$  from the lattice model, represented by circles.

We begin with two vectors  $\mathbf{u}_1 = c_1(-i, -2\alpha, -i)^T$  and  $\mathbf{u}_2 = c_2(0, -i - \alpha, -i)^T$ , where  $c_1 = (2 + 4\alpha^2)^{1/2}$  and  $c_2 = (2 + \alpha^2)^{1/2}$ . This set of vectors yields

$$d_{max} = \sqrt{\frac{3 + 2\alpha^2}{3 + 6\alpha^2}}, \tag{17}$$

where  $\alpha$  can take any real number from  $-\infty$  to  $\infty$ .  $d_{max}$  of the constructed SFB model can take values from  $1/\sqrt{3}$  to 1. Then, we regularize the linearized vector  $\mathbf{v}_{fb} = \mathbf{u}_1 k_1 + \mathbf{u}_2 k_2$  to

$$\mathbf{v}_{fb} = \begin{pmatrix} 1 - \bar{e}_1 \\ -1 + i\alpha\bar{e}_1 + e_2 - i\alpha e_3 \\ \bar{e}_1 - e_2 \end{pmatrix}, \tag{18}$$

where  $e_3 = \bar{e}_1 \bar{e}_2$ . The CLS corresponding to this eigenvector of the flat band is drawn in Fig. 4a by the gray region. From this choice of the CLS, we construct a tight-binding Hamiltonian as follows:

$$H_{kag}(\mathbf{k}) = \begin{pmatrix} g_1 & g_2^* & g_3^* \\ g_2 & 2 & g_4^* \\ g_3 & g_4 & g_1 \end{pmatrix}, \tag{19}$$

where  $g_1 = 2|t|^2$ ,  $g_2 = t(1 + \bar{e}_3)$ ,  $g_3 = t(1 + e_2 + i\alpha t(\bar{e}_1 + e_3))$ ,

$g_4 = t(1 + \bar{e}_1)$ ,  $t = e^{i\theta}\sqrt{1 + \alpha^2}$ , and  $\theta = \cos^{-1}(1/\sqrt{1 + \alpha^2})$ . Note that when  $\alpha = 0$ , where  $d_{max} = 1$ , the model reduces to the kagome lattice model with only nearest-neighbor hopping processes. As the parameter  $\alpha$  grows, the nearest-neighbor hopping parameters become complex-valued, and the next-nearest-neighbor hopping processes are developed as represented by green dashed lines in Fig. 4a. One can assign threading magnetic fluxes corresponding to the complex hopping parameters as illustrated in Fig. 4b, similar to the Haldane model in graphene. In Fig. 4c–e, we plot band dispersions for various values of  $\alpha$ , where we have a zero-energy flat band at the bottom. Fig. 4c) is the well-known band diagram of the kagome lattice with the nearest-neighbor hopping processes. If  $\alpha$  is nonzero, the Dirac point is gapped out due to the broken  $C_6$  symmetry, but the quadratic band-crossing at the  $\Gamma$  point is maintained. We calculate  $d_{max}$  of this model directly using (12) and check that the continuum formula (17) works well as shown in Fig. 4f.

We also construct an SFB tight-binding model in the square lattice bilayer, where one can adjust  $d_{max}$ . The lattice structure is illustrated in Fig. 5a, b, and its band dispersion is plotted in Fig. 5c. As in the kagome lattice case, the construction scheme starts by setting two constant vectors. Our choice is  $\mathbf{u}_1 = c(i\alpha + \gamma, -\alpha - i\gamma)^T$ , and  $\mathbf{u}_2 = \bar{\mathbf{u}}_1$ , where  $c = (2\alpha^2 + 2\gamma^2)^{1/2}$ . One can show



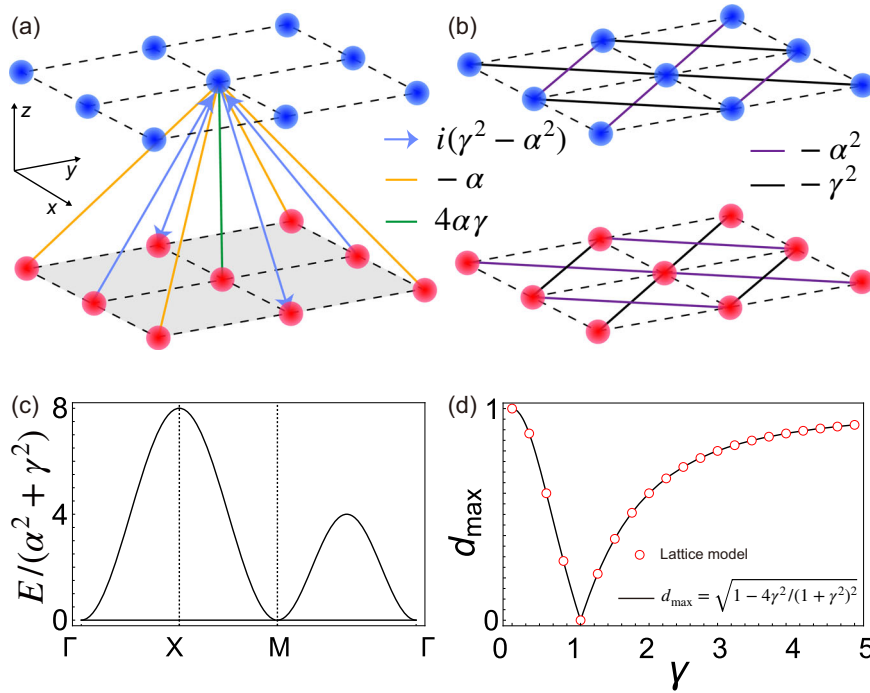


**Fig. 5 The square lattice bilayer model characterized by the quantum distance.** We plot the interlayer and intralayer hopping processes in **a** and **b**, respectively. **c** We plot the band structure, where the energy is scaled by  $\alpha^2 + \gamma^2$ . The relation between the maximum quantum distance  $d_{\max}$  and the band parameter  $\gamma$  is presented in **d**. The results from the lattice model (red circles) are compared with the analytic formula (20) drawn by the solid curve.

that  $d_{\max}$  calculated from these vectors is given by

$$d_{\max} = \sqrt{1 - \frac{4\alpha^2\gamma^2}{(\alpha^2 + \gamma^2)^2}}, \tag{20}$$

where  $\alpha$  and  $\gamma$  can take any real values.  $d_{\max}$  can vary from 0 to 1. If  $\alpha$  or  $\gamma$  is zero

As shown in Fig. 5d,  $d_{\max}$  of the constructed SFB model can take values from 0 to 1. Then, we regularize a vector  $\mathbf{v}_{\text{fb}} = \mathbf{u}_1 k_1 + \mathbf{u}_2 k_2$  to

$$\mathbf{v}_{\text{fb}} = \begin{pmatrix} -i\gamma(1 - e_1 e_2) - \alpha(e_1 - e_2) \\ i\alpha(1 - e_1 e_2) + \gamma(e_1 - e_2) \end{pmatrix}. \tag{21}$$

From this choice of the CLS, we construct a tight-binding Hamiltonian as follows:

$$H_{\text{sq}}(\mathbf{k}) = \begin{pmatrix} |f_2|^2 & f_3 \\ f_3 & |f_1|^2 \end{pmatrix}, \tag{22}$$

where  $f_1 = -i\gamma(1 - e_1 e_2) - \alpha(e_1 - e_2)$ ,  $f_2 = i\alpha(1 - e_1 e_2) + \gamma(e_1 - e_2)$  and  $f_3 = -f_1 \bar{f}_2$ . When  $\alpha = \gamma$  or  $\alpha$  and  $\gamma$  are zero,  $d_{\max} = 1$ . As parameters  $\alpha$  and  $\gamma$  grow, interlayer and intralayer hopping appear, and if  $\alpha \neq \gamma$ , the complex-value hopping process is developed as represented by blue arrow in Fig. 5a. Unlike kagome lattice model, this model has an isotropic band dispersion. As shown in Fig. 5c, the flat band is fixed at the zero energy, and the parabolic band is scaled with  $\alpha^2 + \gamma^2$ . Figure 5d shows  $d_{\max}$  of this model as a function of  $\gamma$ . One calculated by the continuum formula (15) complies with the numerical results from the lattice model evaluated directly from (12).

**Bulk-boundary correspondence.** The bulk-boundary correspondence is the essential idea of the topological analysis of materials<sup>55–62</sup>. Based on this, one can detect the topological information of the bulk by probing the electronic structure of the boundary states. Recently, a new kind of bulk-interface correspondence from the quantum distance for the flat band systems

was developed<sup>43</sup>. Here, a specific type of interface is considered, which is generated between two domains of an SFB system with different onsite potentials  $U_R$  and  $U_L$ . Note that the two domains are characterized by the same geometric quantity  $d_{\max}$ , unlike the topological bulk-boundary correspondence, where the boundary is formed between two regions with different topological characters. In the case of the SFB systems, an interface state is guaranteed to exist if the value of  $d_{\max}$  is nonzero, and the corresponding band dispersion around the band-crossing point is given by

$$E_{\text{IF}}(k) \approx \frac{d_{\max}^2}{2m_b} k^2 + U_0, \tag{23}$$

where  $k$  and  $m_b$  are the crystal momentum and the bulk mass along the direction of the interface, respectively, and  $U_0 = \min(U_R, U_L)$ . This formula implies that the effective mass of the interface mode is  $m^* = m_b/d_{\max}^2$ .

Now, we examine the formula (23) for the finite systems satisfying the open boundary condition. In the previous work, (23) could be obtained by presuming an exponentially decaying edge mode, and the existence of such a state was guaranteed for the specific interface of the step-like potential. While the open boundaries are naturally induced when we prepare a sample, the application of the step-like potential is not usually straightforward in experiments. Therefore, it is worthwhile to investigate the bulk-boundary correspondence for the open boundary systems. In the case of the open boundary, the bulk-boundary correspondence states that if edge-localized modes exist, their energy spectrum is given by (23). Note that the edge modes are not guaranteed to appear within the open boundary condition. For example, the modified Lieb lattice model yields an interface mode when there is a chemical potential difference over the system as studied in reference [43], while we do not have an edge mode under the open boundary condition [See Supplementary Fig. 1 in Supplementary Note 3].

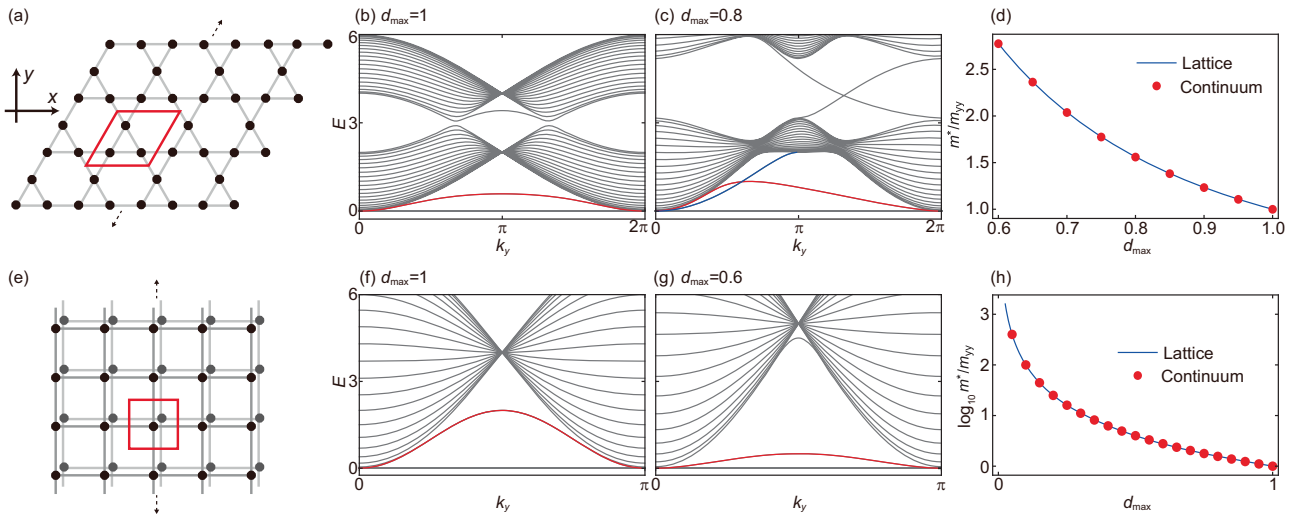


**Fig. 6 The Bulk-boundary correspondence of singular flat band systems.** **a** The lattice structure of the kagome lattice model. The unit cell is indicated by the red box. **b, c** are the band structures of the kagome lattice model with  $W = 20$  for various values of the maximum quantum distance  $d_{\max}$ . **d** We plot the effective mass of the boundary modes of the kagome lattice model around  $k_y = 0$  as a function of  $d_{\max}$  and compare it with the continuum result (red circles) in (23). **e** The lattice structure of the square lattice bilayer model, where the red box represents the unit cell. **f, g** We plot the band spectra of the square lattice bilayer model with  $W = 20$  for various values of  $d_{\max}$ . **h** The  $d_{\max}$ -dependence of the effective mass of the boundary modes of the square lattice bilayer around  $k_y = 0$ . The general continuum formula (23) of the effective mass is drawn by red circles.

We first consider the kagome lattice model. We note that boundary modes exist for the ribbon geometry of this system illustrated in Fig. 6a, which respects the translational symmetry along  $(1/2, \sqrt{3}/2)$  while terminated along the  $x$  axis. The width  $W$  of the kagome ribbon is defined as the number of the unit cells along the  $x$  axis. For example, the width of the kagome ribbon shown in Fig. 6a is 4. We plot the band dispersions of the kagome ribbons with  $W = 20$  for  $d_{\max} = 1$  and  $d_{\max} = 0.8$  in Fig. 6b, c, respectively. The red and blue lines represent the boundary modes stemming from the band-crossing point at  $k_y = 0$ . While the band dispersions of the left (near  $k_y \approx 0$ )- and right (near  $k_y \approx 2\pi$ )-localized modes in Fig. 6b are precisely the same for the  $d_{\max} = 1$  case, it is not for  $0 < d_{\max} < 1$  case due to the broken time-reversal symmetry. For this reason, we distinguish the left- and right-localized modes by the red and blue colors in Fig. 6c. We check that the blue and red curves, although they look asymmetric with respect to  $k_y = 0$ , they follow the same parabolic equation (23) in the vicinity of the touching point at  $k_y = 0$  [See Supplementary Fig. 2 in Supplementary Note 4]. We numerically calculate the effective mass of the boundary modes from the kagome lattice model and compare it with the analytic result of the effective mass  $m^* = m_b/d_{\max}^2$  in (23). As plotted in Fig. 6d, the formula (23) describes the numerical results perfectly for any values of  $d_{\max}$ . Second, we also investigate the edge state of the square lattice bilayer ribbon shown in Fig. 6e. As in the kagome model, the width  $W$  of this system is defined as the number of unit cells along the  $x$  axis. In Fig. 6f, g, we plot the band structures of the square lattice bilayer ribbon with  $W = 20$ . The red curves, which are doubly degenerate, correspond to the boundary modes. We confirm that the effective mass of the boundary modes obeys the continuum formula (23) well as plotted in Fig. 6h.

## Discussion

In summary, we propose a construction scheme for tight-binding Hamiltonians hosting a flat band whose band-touching point is characterized by  $d_{\max}$ , the maximum value of the quantum distance between Bloch eigenstates around the touching point. Based on the scheme, we built several flat band tight-binding models with simple hopping structures in the kagome lattice and the

square lattice bilayer, where one can control  $d_{\max}$ . We note that complex and long-range (at least the next-nearest ones) hopping amplitudes are necessary to change  $d_{\max}$  between 0 and 1. This implies that the candidate materials hosting an SFB with  $0 < d_{\max} < 1$  could be found among the materials with strong spin-orbit coupling. We believe that our construction scheme could inspire the material search for geometrically nontrivial flat band systems. If we extend the category of the materials to the artificial systems, our lattice models with the fine-tuned complex hopping parameters are expected to be realized in the synthetic dimensions<sup>63–69</sup> and circuit lattices<sup>70,71</sup>. Then, we propose a bulk-boundary correspondence between the bulk number  $d_{\max}$  and the shape of the low-energy dispersion of the boundary modes within the open boundary condition. The information of  $d_{\max}$  is embedded in the effective mass of the band dispersion of the edge states. This correspondence provides us with a tool to detect  $d_{\max}$  from the spectroscopy of the finite SFB systems. Notably, the bulk-boundary correspondence is obtained from the continuum Hamiltonian around the band-crossing point. This implies that even if the flat band obtained from our construction scheme is slightly deformed in real systems, one can investigate the geometric properties of the SFB. It is worthwhile to remark that the  $d_{\max}$ -driven bulk-boundary correspondence is distinguished from the conventional one in that the former predicts the effective mass of the interface mode instead of its existence.

## Method

**A condition for the CLS to have a noninteger  $d_{\max}$ .** In this section, we show that at least one component of  $\alpha_{\mathbf{k}}\mathbf{v}_{\mathbf{k}}$ , the Fourier transform of the CLS, should contain more than two different exponential factors  $e^{-i(mq_1+nq_2)}$ . Here,  $q_i$  is the momentum with respect to the band-crossing point, and  $m$  and  $n$  are integer numbers. To this end, we verify that if all the components of  $\alpha_{\mathbf{k}}\mathbf{v}_{\mathbf{k}}$  have two or less than two exponential factors,  $d_{\max}$  of the corresponding flat band is one or zero. The  $q$ -th component of such an eigenvector can be written as

$$\alpha_{\mathbf{k}}\mathbf{v}_{\mathbf{k}}|_q = A_{m_1, n_1} e^{-i(m_1 q_1 + n_1 q_2)} + A_{m_2, n_2} e^{-i(m_2 q_1 + n_2 q_2)}. \quad (24)$$

Since we assume that the flat band is singular at the band-

touching point, the coefficients satisfy

$$A_{m_1, n_1} + A_{m_2, n_2} = 0. \quad (25)$$

As a result, the linear expansion of  $\alpha_{\mathbf{k}}$  becomes

$$\alpha_{\mathbf{k}} \mathbf{v}_{\mathbf{k}}|_q \approx -iA_{m_1, n_1} [(m_1 - m_2)q_1 - (n_1 - n_2)q_1], \quad (26)$$

leading to  $u_{1,q}^* u_{2,q} = |A_{m_1, n_1}|^2 (m_1 - m_2)(n_1 - n_2)$ , where  $u_{i,q}$  is the  $q$ -th component of  $\mathbf{u}_i$  defined in (14). Therefore,  $\mathbf{u}_1^* \cdot \mathbf{u}_2 = \sum_q u_{1,q}^* u_{2,q}$  is a real number, which proves the statement at the beginning of this section. Namely, we need at least three different exponential factors in at least one component of  $\alpha_{\mathbf{k}}$ .

### Data availability

Data sharing is not applicable.

### Code availability

Code sharing is not applicable.

Received: 9 May 2023; Accepted: 28 September 2023;

Published online: 18 October 2023

### References

- Leykam, D., Andreanov, A. & Flach, S. Artificial flat band systems: from lattice models to experiments. *Adv. Phys.: X* **3**, 1473052 (2018).
- Rhim, J.-W. & Yang, B.-J. Singular flat bands. *Adv. Phys.: X* **6**, 1901606 (2021).
- Volovik, G. The fermi condensate near the saddle point and in the vortex core. *JETP Lett.* **59**, 830 (1994).
- Cao, Y. et al. Unconventional superconductivity in magic-angle graphene superlattices. *Nature* **556**, 43–50 (2018).
- Liu, X. et al. Spectroscopy of a tunable moiré system with a correlated and topological flat band. *Nat. Commun.* **12**, 1–7 (2021).
- Balents, L., Dean, C. R., Efetov, D. K. & Young, A. F. Superconductivity and strong correlations in moiré flat bands. *Nat. Phys.* **16**, 725–733 (2020).
- Peri, V., Song, Z.-D., Bernevig, B. A. & Huber, S. D. Fragile topology and flat-band superconductivity in the strong-coupling regime. *Phys. Rev. Lett.* **126**, 027002 (2021).
- Yudin, D. et al. Fermi condensation near van hove singularities within the hubbard model on the triangular lattice. *Phys. Rev. Lett.* **112**, 070403 (2014).
- Volovik, G. E. Graphite, graphene, and the flat band superconductivity. *JETP Lett.* **107**, 516–517 (2018).
- Aoki, H. Theoretical possibilities for flat band superconductivity. *J. Supercond. Nov. Magn.* **33**, 2341–2346 (2020).
- Kononov, A. et al. Superconductivity in type-ii weyl-semimetal wte2 induced by a normal metal contact. *J. Appl. Phys.* **129**, 113903 (2021).
- Mielke, A. Ferromagnetism in the hubbard model and hund's rule. *Phys. Lett. A* **174**, 443–448 (1993).
- Tasaki, H. From nagaoka's ferromagnetism to flat-band ferromagnetism and beyond: an introduction to ferromagnetism in the hubbard model. *Prog. Theor. Phys.* **99**, 489–548 (1998).
- Mielke, A. Stability of ferromagnetism in hubbard models with degenerate single-particle ground states. *J. Phys. A* **32**, 8411 (1999).
- Hase, I., Yanagisawa, T., Aiura, Y. & Kawashima, K. Possibility of flat-band ferromagnetism in hole-doped pyrochlore oxides  $\text{Sn}_2\text{Nb}_2\text{O}_7$  and  $\text{S}_2\text{Ta}_2\text{O}_7$ . *Phys. Rev. Lett.* **120**, 196401 (2018).
- You, J.-Y., Gu, B. & Su, G. Flat band and hole-induced ferromagnetism in a novel carbon monolayer. *Sci. Rep.* **9**, 1–7 (2019).
- Saito, Y. et al. Hofstadter subband ferromagnetism and symmetry-broken chern insulators in twisted bilayer graphene. *Nat. Phys.* **17**, 478–481 (2021).
- Sharpe, A. L. et al. Emergent ferromagnetism near three-quarters filling in twisted bilayer graphene. *Science* **365**, 605–608 (2019).
- Wu, C., Bergman, D., Balents, L. & Sarma, S. D. Flat bands and wigner crystallization in the honeycomb optical lattice. *Phys. Rev. Lett.* **99**, 070401 (2007).
- Chen, Y. et al. Ferromagnetism and wigner crystallization in kagome graphene and related structures. *Phys. Rev. B* **98**, 035135 (2018).
- Jaworowski, B. et al. Wigner crystallization in topological flat bands. *New J. Phys.* **20**, 063023 (2018).
- Wang, F. & Ran, Y. Nearly flat band with chern number  $c = 2$  on the dice lattice. *Phys. Rev. B* **84**, 241103 (2011).
- Tang, E., Mei, J.-W. & Wen, X.-G. High-temperature fractional quantum hall states. *Phys. Rev. Lett.* **106**, 236802 (2011).
- Sun, K., Gu, Z., Katsura, H. & Sarma, S. D. Nearly flatbands with nontrivial topology. *Phys. Rev. Lett.* **106**, 236803 (2011).
- Neupert, T., Santos, L., Chamon, C. & Mudry, C. Fractional quantum hall states at zero magnetic field. *Phys. Rev. Lett.* **106**, 236804 (2011).
- Sheng, D., Gu, Z.-C., Sun, K. & Sheng, L. Fractional quantum hall effect in the absence of landau levels. *Nat. Commun.* **2**, 1–5 (2011).
- Regnault, N. & Bernevig, B. A. Fractional chern insulator. *Phys. Rev. X* **1**, 021014 (2011).
- Weeks, C. & Franz, M. Flat bands with nontrivial topology in three dimensions. *Phys. Rev. B* **85**, 041104 (2012).
- Yang, S., Gu, Z.-C., Sun, K. & Sarma, S. D. Topological flat band models with arbitrary chern numbers. *Phys. Rev. B* **86**, 241112 (2012).
- Liu, Z., Bergholtz, E. J., Fan, H. & Läuchli, A. M. Fractional chern insulators in topological flat bands with higher chern number. *Phys. Rev. Lett.* **109**, 186805 (2012).
- Bergholtz, E. J. & Liu, Z. Topological flat band models and fractional chern insulators. *Int. J. Mod. Phys. B* **27**, 1330017 (2013).
- Rhim, J.-W., Kim, K. & Yang, B.-J. Quantum distance and anomalous landau levels of flat bands. *Nature* **584**, 59–63 (2020).
- Hwang, Y., Rhim, J.-W. & Yang, B.-J. Geometric characterization of anomalous landau levels of isolated flat bands. *Nat. Commun.* **12**, 1–9 (2021).
- Peotta, S. & Törmä, P. Superfluidity in topologically nontrivial flat bands. *Nat. Commun.* **6**, 8944 (2015).
- Törmä, P., Peotta, S. & Bernevig, B. A. Superconductivity, superfluidity and quantum geometry in twisted multilayer systems. *Nat. Rev. Phys.* **4**, 528–542 (2022).
- Piéchon, F., Raoux, A., Fuchs, J.-N. & Montambaux, G. Geometric orbital susceptibility: quantum metric without berry curvature. *Phys. Rev. B* **94**, 134423 (2016).
- Bužek, V. & Hillery, M. Quantum copying: beyond the no-cloning theorem. *Phys. Rev. A* **54**, 1844 (1996).
- Dodonov, V., Man'Ko, O., Man'Ko, V. & Wünsche, A. Hilbert-schmidt distance and non-classicality of states in quantum optics. *J. Mod. Opt.* **47**, 633–654 (2000).
- Wilczek, F. & Shapere, A. Geometric phases in physics, vol. 5 (World Scientific, 1989).
- Rhim, J.-W. & Yang, B.-J. Classification of flat bands according to the band-crossing singularity of bloch wave functions. *Phys. Rev. B* **99**, 045107 (2019).
- Bergman, D. L., Wu, C. & Balents, L. Band touching from real-space topology in frustrated hopping models. *Phys. Rev. B* **78**, 125104 (2008).
- Ma, J. et al. Direct observation of flatband loop states arising from nontrivial real-space topology. *Phys. Rev. Lett.* **124**, 183901 (2020).
- Oh, C.-g., Cho, D., Park, S. Y. & Rhim, J.-W. Bulk-interface correspondence from quantum distance in flat band systems. *Communications Physics* **5**, 320 (2022).
- Mizoguchi, T. & Udagawa, M. Flat-band engineering in tight-binding models: beyond the nearest-neighbor hopping. *Phys. Rev. B* **99**, 235118 (2019).
- Călugăru, D. et al. General construction and topological classification of crystalline flat bands. *Nat. Phys.* **18**, 185–189 (2022).
- Mizoguchi, T. & Hatsugai, Y. Systematic construction of topological flat-band models by molecular-orbital representation. *Phys. Rev. B* **101**, 235125 (2020).
- Graf, A. & Piéchon, F. Designing flat-band tight-binding models with tunable multifold band touching points. *Phys. Rev. B* **104**, 195128 (2021).
- Hwang, Y., Jung, J., Rhim, J.-W. & Yang, B.-J. Wave-function geometry of band crossing points in two dimensions. *Phys. Rev. B* **103**, L241102 (2021).
- Hwang, Y., Rhim, J.-W. & Yang, B.-J. Flat bands with band crossings enforced by symmetry representation. *Phys. Rev. B* **104**, L081104 (2021).
- Hwang, Y., Rhim, J.-W. & Yang, B.-J. General construction of flat bands with and without band crossings based on wave function singularity. *Phys. Rev. B* **104**, 085144 (2021).
- Maimaiti, W., Flach, S. & Andreanov, A. Universal  $d = 1$  flat band generator from compact localized states. *Phys. Rev. B* **99**, 125129 (2019).
- Huda, M. N., Kezilebieke, S. & Liljeroth, P. Designer flat bands in quasi-one-dimensional atomic lattices. *Phys. Rev. Res.* **2**, 043426 (2020).
- Rhim, J.-W., Behrends, J. & Bardarson, J. H. Bulk-boundary correspondence from the intercellular zak phase. *Phys. Rev. B* **95**, 035421 (2017).
- Provost, J. P. & Vallee, G. Riemannian structure on manifolds of quantum states. *Commun. Math. Phys.* **76**, 289 (1980).
- Kane, C. L. & Mele, E. J. Quantum spin hall effect in graphene. *Phys. Rev. Lett.* **95**, 226801 (2005).
- Kane, C. L. & Mele, E. J. Z 2 topological order and the quantum spin hall effect. *Phys. Rev. Lett.* **95**, 146802 (2005).
- Bernevig, B. A. & Zhang, S.-C. Quantum spin hall effect. *Phys. Rev. Lett.* **96**, 106802 (2006).



58. Hatsugai, Y. Chern number and edge states in the integer quantum hall effect. *Phys. Rev. Lett.* **71**, 3697 (1993).
59. Kitaev, A. Periodic table for topological insulators and superconductors. In: *ALP conference proceedings*, vol. **1134**, 22–30 (American Institute of Physics, 2009).
60. Fukui, T., Shiozaki, K., Fujiwara, T. & Fujimoto, S. Bulk-edge correspondence for chern topological phases: a viewpoint from a generalized index theorem. *J. Phys. Soc. Jpn.* **81**, 114602 (2012).
61. Mong, R. S. & Shivamoggi, V. Edge states and the bulk-boundary correspondence in dirac hamiltonians. *Phys. Rev. B* **83**, 125109 (2011).
62. Rhim, J.-W., Bardarson, J. H. & Slager, R.-J. Unified bulk-boundary correspondence for band insulators. *Phys. Rev. B* **97**, 115143 (2018).
63. Celi, A. et al. Synthetic gauge fields in synthetic dimensions. *Phys. Rev. Lett.* **112**, 043001 (2014).
64. Ozawa, T. & Price, H. M. Topological quantum matter in synthetic dimensions. *Nat. Rev. Phys.* **1**, 349–357 (2019).
65. Yuan, L., Lin, Q., Xiao, M. & Fan, S. Synthetic dimension in photonics. *Optica* **5**, 1396–1405 (2018).
66. Dutt, A. et al. Experimental band structure spectroscopy along a synthetic dimension. *Nat. Commun.* **10**, 3122 (2019).
67. Balčytis, A. et al. Synthetic dimension band structures on a si cmos photonic platform. *Sci. Adv.* **8**, eabk0468 (2022).
68. Ozawa, T., Price, H. M., Goldman, N., Zilberberg, O. & Carusotto, I. Synthetic dimensions in integrated photonics: from optical isolation to four-dimensional quantum hall physics. *Phys. Rev. A* **93**, 043827 (2016).
69. Ozawa, T. & Carusotto, I. Synthetic dimensions with magnetic fields and local interactions in photonic lattices. *Phys. Rev. Lett.* **118**, 013601 (2017).
70. Albert, V. V., Glazman, L. I. & Jiang, L. Topological properties of linear circuit lattices. *Phys. Rev. Lett.* **114**, 173902 (2015).
71. Kim, Y. et al. Realization of non-hermitian hopf bundle matter. *arXiv* <https://arxiv.org/abs/2303.13721> (2023).

## Acknowledgements

This work was supported by the National Research Foundation of Korea (NRF) Grant funded by the Korean government (MSIT) (Grant no. 2021R1A2C1010572 and 2021R1A5A1032996 and 2022M3H3A106307411).

## Author contributions

H.K. and C.-g.O. contributed equally to this work. H.K. developed the general flat band construction scheme. C.-g.O. performed the theoretical analysis of the bulk-boundary correspondence. J.W.R. supervised the project.

## Competing interests

The authors declare no competing interests.

## Additional information

**Supplementary information** The online version contains supplementary material available at <https://doi.org/10.1038/s42005-023-01407-6>.

**Correspondence** and requests for materials should be addressed to Jun-Won Rhim.

**Peer review information** *Communications Physics* thanks Alexei Andreanov, Aleksandra Maluckov, and the other, anonymous, reviewer (s) for their contribution to the peer review of this work. A peer review file is available.

**Reprints and permission information** is available at <http://www.nature.com/reprints>

**Publisher's note** Springer Nature remains neutral with regard to jurisdictional claims in published maps and institutional affiliations.



**Open Access** This article is licensed under a Creative Commons Attribution 4.0 International License, which permits use, sharing, adaptation, distribution and reproduction in any medium or format, as long as you give appropriate credit to the original author(s) and the source, provide a link to the Creative Commons licence, and indicate if changes were made. The images or other third party material in this article are included in the article's Creative Commons licence, unless indicated otherwise in a credit line to the material. If material is not included in the article's Creative Commons licence and your intended use is not permitted by statutory regulation or exceeds the permitted use, you will need to obtain permission directly from the copyright holder. To view a copy of this licence, visit <http://creativecommons.org/licenses/by/4.0/>.

© The Author(s) 2023